24th COBEM - 2017

24th ABCM International Congress of Mechanical Engineering
December 3-8, 2017, Curitiba, PR, Brazil

COBEM-2017-2071
NUMERICAL AND EXPERIMENTAL ANALYSIS OF A CRACKED SHAFT BASED ON STATIC AND DYNAMIC RESPONSES

Izabela Batista da Silva
Tobias Souza Morais
Aldemir Ap Cavalini Jr
Valder Steffen Jr
LMEst - Structural Mechanics Laboratory, Federal University of Uberlândia, School of Mechanical Engineering, Av. João Naves de Ávila, 2121, Uberlândia, MG, 38408-196, Brazil, izabela.silva@ufu.br.

Abstract. *Monitoring techniques devoted to rotating machinery are important tools used to provide safety operation conditions to these systems. Vibration based monitoring approaches are commonly used for crack detection in rotating shafts due to their ability to evaluate small changes in the physical parameters of the system. In this context, this paper aims at evaluating the effects of a transverse crack on a shaft-bearing test rig both from numerical and experimental results. The existence of a crack in the shaft introduces an additional flexibility, which is determined by using the strain energy density criterion and the linear fracture mechanics theory. This additional flexibility is taken into account from static and dynamic analyzes, in which a 2D finite element model of the shaft with an open crack is used. Additionally, a 3D non-linear model is formulated in the same conditions for comparison purposes. As a result, natural frequencies and strain measures of the healthy and cracked shaft are compared.*

Keywords: *rotating machines, monitoring technique, crack behavior, 2D and 3D finite element models.*

1. INTRODUCTION

Damage in mechanical systems is associated to changes either in material or geometric properties, causing adverse effects in the system performance. Cracks in shafts of rotating machines lead to geometric discontinuities, which affect physical properties of the machine. According to the crack severity and the amplitude of the applied load, catastrophic failure may happen (Farrar, 2005). Thus, the detection of incipient cracks and the prediction of its growth are able to avoid unnecessary machine downtime. If the monitoring is effective, a better utilization of the machines is also obtained (Muszynska, 2005).

Dynamic tests based on vibration measurements are widely used to crack detection in rotating machines. Cracks reduce the stiffness of the shaft locally, which causes a change in the dynamic behavior of the system (Bachschmid, *et al.*, 2010). The influence of transversal cracks on the dynamic behavior of rotating shafts is a topic largely covered in the literature, which is the aim of the present paper.

Several works proposed mathematical models to represents the effects of cracks both on the static and dynamic behavior of rotating shafts by using different formulations. Cracks with breathing behavior are presented in Gasch (1976), Mayes and Davies (1984), and Bachschmid et al. (2010). These models take into account the opening and closure behavior of the crack. Al-Shudeifat (2013) proposed an open crack model based on the advanced phase of the breathing crack. Dimarogonas (1996) applied the linear fracture mechanics theory (considering the strain energy release rate, the stress intensification factors, and the Castiglione theorem) to determine the local flexibility introduced in the shaft by a crack. Different formulations concerning the additional flexibility matrix and the coupling between lateral, longitudinal, and torsional vibrations are shown in Papadopoulos and Dimarogonas (1987), Papadopoulos and Dimarogonas (1989), Ostachowicz (1992) and Darpe *et al.* (2004).

In this context, the present work aims at evaluating the dynamic behavior of a cracked shaft through numerical and experimental investigations. Thus, the results obtained from static and dynamic analysis considering 2D and 3D models are compared with experimental measurements. In this case, the strain field around the crack region is measured for different crack depths. The crack is considered always open, independently of the shaft angular position. The numerical and experimental natural frequencies of the healthy and cracked shaft are also compared based on measures of the frequency response functions (FRFs) of the system.

2. EXPERIMENTAL PROCEDURE

For the analysis considered in this work, a shaft-bearing-disc system is assembled like a cantilever beam as presented in Fig. 1. It is composed of a flexible steel shaft with 1005 mm length and 17 mm diameter (E = 205 GPa, ρ = 7850 kg/m^3, ν = 0.29), one rigid disc with 150 mm diameter and 20 mm thickness (ρ = 7850 kg/m^3), and two roller bearings. The bearing stiffness and damping coefficients were determined by solving a typical inverse problem using the heuristic optimization technique Differential Evolution (Storn and Price, 1995).

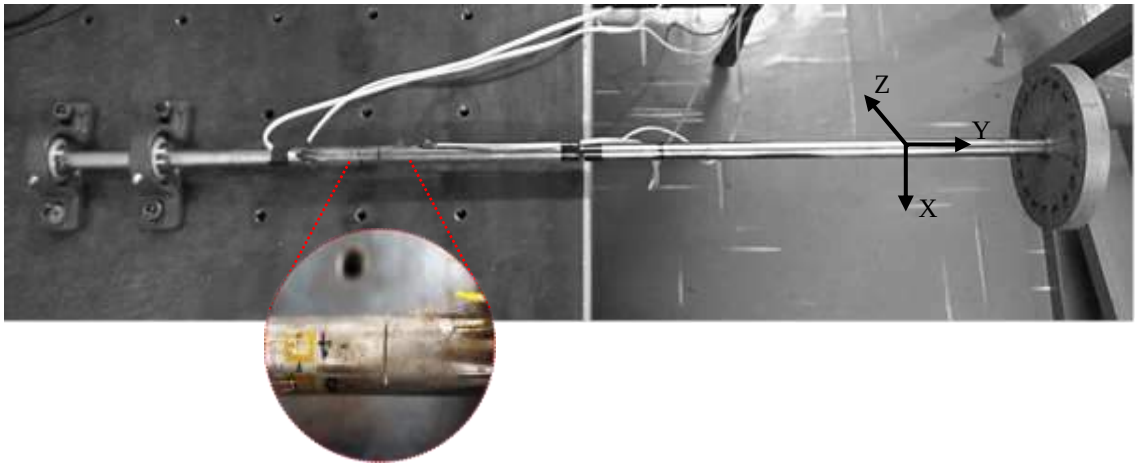

Figure 1. Shaft-bearing-disc test rig used for experimental analysis

In the experimental procedure, six strain gages were used to measure the strain fields close to the crack location at 310 and 340 mm from the bearing (see Fig. 1). The strain-gauge positions are shown in Fig. 2.

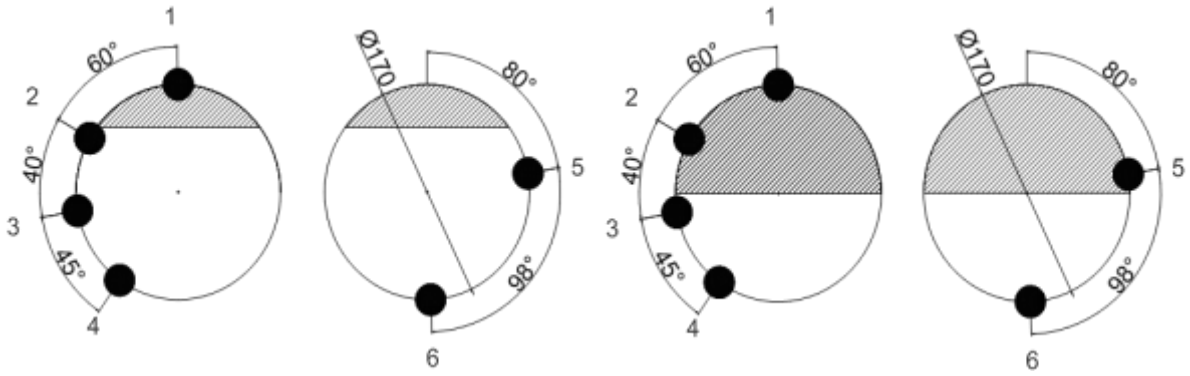

Figure 2. Strain gauges positions for (a) 20% depth transversal crack. (b) 50% depth transversal crack.

The ADS2000 data acquisition system is used to measure the associated strain fields. Experimental FRFs were measured by applying impact forces along the X and Z directions of the disc (see Fig. 1). Then, vibration responses were obtained through an accelerometer positioned at the disc along the same direction of the impact forces, resulting two FRFs. The measurements were performed by using the signal analyzer Agilent (model 35670A) in a range of 0-100 Hz and steps of 0.25 Hz.

3. 2D MODEL

The 2D finite element model was formulated based on the Timoshenko's beam theory. It is assumed that shaft is flexible and the disc is rigid.

The shaft element with two nodes and 4 degrees of freedom per node (u, W, θ, φ) was considered as shows Fig. 3.

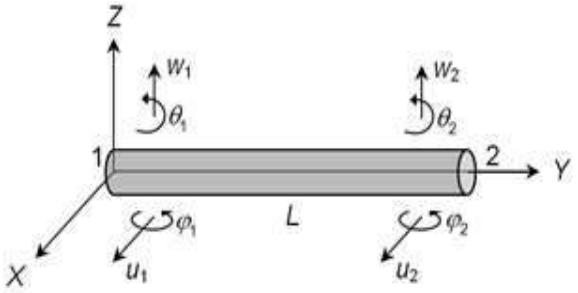

Figure 3. Timoshenko beam element with 8 degrees of freedom

Figure 4 shows the shaft-bearing-disc system formulated with 38 beam elements. The crack location is assumed to be at the element #14 (between the nodes #14 and #15). The two roller bearings are located at the nodes #2 and #6. The disc is located at the node #37. The geometric and physical properties used to formulate the finite element model of the experimental test rig were given in section 2.

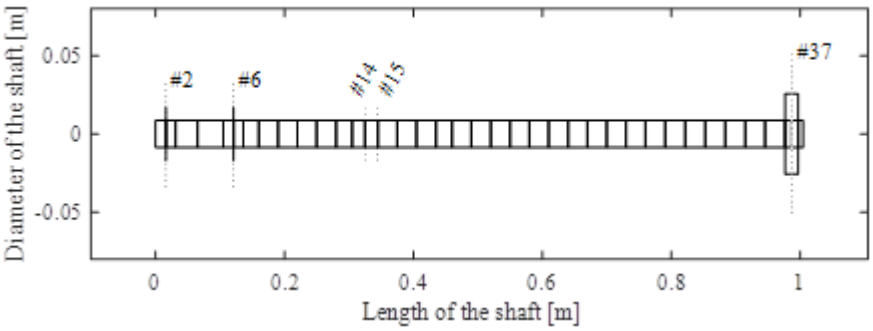

Figure 4. Shaft-bearing-disc finite element model

The dynamic behavior of cracked flexible shaft supported by roller bearings is represented mathematically as shown by Eq. (1).

$$\boldsymbol{M}\ddot{\boldsymbol{q}} + \boldsymbol{D}\dot{\boldsymbol{q}} + \boldsymbol{K}(\Omega t)\boldsymbol{q} = \boldsymbol{W} \tag{1}$$

where $\boldsymbol{M}$ is the mass matrix, $\boldsymbol{D}$ is the damping matrix, $\boldsymbol{K}(\Omega t)$ is the stiffness matrix with variable values due to the crack (i.e., Ωt stands to the angular position of the shaft), $\boldsymbol{W}$ stands for the weight of the rotating parts, and $\boldsymbol{q}$ is the generalized displacement vector. The numerical FRFs (2D model) were determined from the solution of the equations of motion directly in the frequency domain.

Regarding the crack simulation, the dynamic model of the finite element with a crack is obtained by using first the linear fracture mechanics theory to determine the additional flexibility produced by the crack. This formulation is explained next, assuming a beam element containing a transverse crack with depth α, as shows Fig. 5.

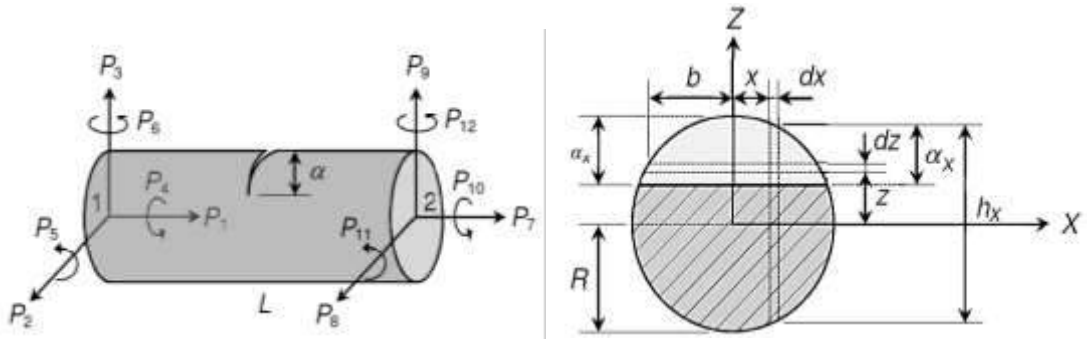

(a) (b)

Figure 5: (a) Shaft element with a crack. (b) Details about the cross-section of the crack element

The Castiglione theorem is used to determine the cracked shaft displacement u_i in the direction of the load P_i, as presents the Eq. (2) (Darpe et al., 2004).

$$u_i = \frac{dU}{dP_i} = \frac{\partial U^0}{\partial P_i} + \frac{\partial U^c}{\partial P_i} \tag{2}$$

where U^0 is the elastic strain energy of the shaft element with crack and U^c is the additional strain energy due to the crack presence, as described by Eq. (3) and Eq. (4), respectively, in which the concepts of fracture mechanics are used.

$$U^0 = \frac{1}{2}\left[\frac{P_1^2 L}{AE} + \frac{\alpha_s P_2^2 L}{GA} + \frac{P_2^2 L^3}{3EI} + \frac{\alpha_s P_3^2 L}{GA} + \frac{P_3^2 L^3}{3EI} + \frac{P_4^2 L}{GI_0} + \frac{P_5^2 L}{EI} + \frac{P_6^2 L}{EI} + \frac{P_2 P_6 L^2}{EI} + \frac{P_3 P_5 L^2}{EI}\right] \tag{3}$$

$$U^c = \int_A J(A)\,dA = \int_A \frac{1-\upsilon}{E}\left[\left(\sum_{i=1}^{6} K_{Ii}\right)^2 + \left(\sum_{i=1}^{6} K_{IIi}\right)^2 + (1+\upsilon)\left(\sum_{i=1}^{6} K_{IIIi}\right)^2\right] \tag{4}$$

where E is the Young's modulus, v is the Poisson's ratio, G is the shear modulus, I is the area moment of inertia, and I_0 is the polar moment of inertia. K_{Ii}, K_{IIi}, and K_{IIIi} are the stress intensity factors (SIF). In this case, where the principal load is applied normal to the crack plane, only the crack load mode K_{Ii} is considered (Anderson, 2005). The SIF are shown in Eq. (5).

$$K_{mi} = Y\sigma_i\sqrt{\pi\alpha} \tag{5}$$

where K_{mi} is the SIF (I, II or III), σ_i is the stress distribution on the crack, and Y are the shape functions. The additional flexibility c_{ij} is obtained as exposed in Eq. (6).

$$c_{ij} = \frac{\partial^2 U^c}{\partial P_i \partial P_j} \tag{6}$$

where the resulting integrals were calculated by using the procedure described in Papadopoulos (2004). Therefore, the additional flexibility matrix due to the crack is given by the Eq. (7).

$$\boldsymbol{c} = \begin{bmatrix} 0 & 0 & 0 & 0 \\ & 0 & 0 & 0 \\ & & c_{55} & c_{56} \\ sim. & & & c_{66} \end{bmatrix} \tag{7}$$

Equation (8) shows that the additional flexibility matrix due to the crack is included on the flexibility matrix of the uncracked shaft ($\boldsymbol{c_0}$) to obtain the resulting flexibility of the shaft element with the crack.

$$\boldsymbol{c_{CE}} = \boldsymbol{c_0} + \boldsymbol{c} \tag{8}$$

Equation (9) presents the stiffness coefficients k_ξ and k_η that are obtained from the inverse value of $\boldsymbol{c_{CE}}$ ($k_\xi = \boldsymbol{c_{CE}}^{-1}$ (1,1), $k_\eta = \boldsymbol{c_{CE}}^{-1}$ (2,2)), which are used tor determine the stiffness of the shaft with crack in fixed coordinates $\boldsymbol{K_F}$. Note that $\boldsymbol{K_F}$ changes according to the angular position of the shaft.

$$\boldsymbol{K_F} = \begin{bmatrix} cos(\theta) & -sin(\theta) \\ sin(\theta) & cos(\theta) \end{bmatrix}\begin{bmatrix} k_\xi & 0 \\ 0 & k_\eta \end{bmatrix}\begin{bmatrix} cos(\theta) & sin(\theta) \\ -sin(\theta) & cos(\theta) \end{bmatrix} \tag{9}$$

where θ is the angular position of the shaft ($\theta = \Omega t$).

Finally, the stiffness matrix of the shaft element with the transverse crack $\boldsymbol{K_{CE}}$ is calculated by a combination of the matrices shown in Eq. (10) and Eq. (11) as follows:

$$\boldsymbol{K}_{XY} = \frac{12EI}{L^3\left(1+\vartheta_Y\right)}\begin{bmatrix} -1 & 0 \\ L & -1 \\ 1 & 0 \\ 0 & 1 \end{bmatrix}\begin{bmatrix} K_F(1,1) & \frac{L}{2} \\ \frac{L}{2} & \frac{\left(4+\vartheta_Y\right)}{12}L^2 \end{bmatrix}\begin{bmatrix} -1 & L & 1 & 0 \\ 0 & -1 & 0 & 1 \end{bmatrix} \tag{10}$$

$$\boldsymbol{K}_{YZ} = \frac{12EI}{L^3\left(1+\vartheta_Y\right)}\begin{bmatrix} -1 & 0 \\ -L & -1 \\ 1 & 0 \\ 0 & 1 \end{bmatrix}\begin{bmatrix} K_F(2,2) & -\frac{L}{2} \\ -\frac{L}{2} & \frac{\left(4+\vartheta_Y\right)}{12}L^2 \end{bmatrix}\begin{bmatrix} -1 & -L & 1 & 0 \\ 0 & -1 & 0 & 1 \end{bmatrix} \tag{11}$$

4. COMPUTATIONAL PROCEDURE - 3D MODEL

The 3D model of the shaft-bearing-disc test rig was developed by using the software ANSYS®. Figure 6 shows the formulated model according to the geometry and parameters presented earlier in section 2.

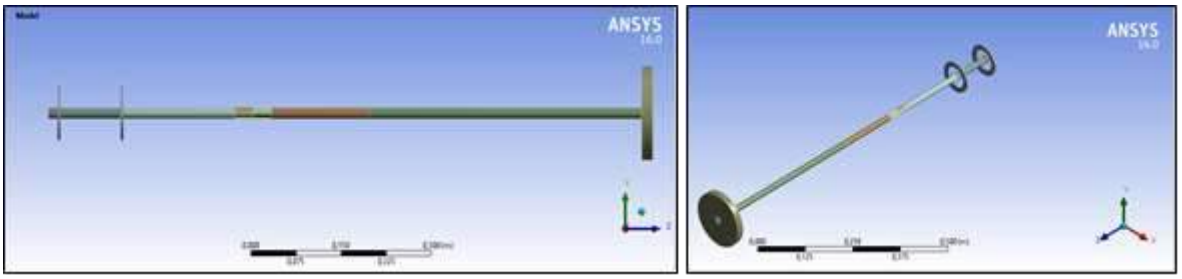

Figure 6. 3D model developed in Ansys®

The bearings are represented by two connections *Ground to Multiple* type and a mesh refinement was used in the crack region considering a 0.001 mm element size for representativeness purposes.

5. RESULTS AND DISCUSSION

Figure 7 presents the numerical (updated 2D model) and experimental FRFs obtained considering the healthy shaft configuration. The FRFs were obtained from impact forces performed at the disc along the *X* and *Z* directions (Fig. 7a and Fig. 7b, respectively). Note that the results are very similar, i.e., the 2D model is able to represent the dynamic behavior of the system, satisfactorily.

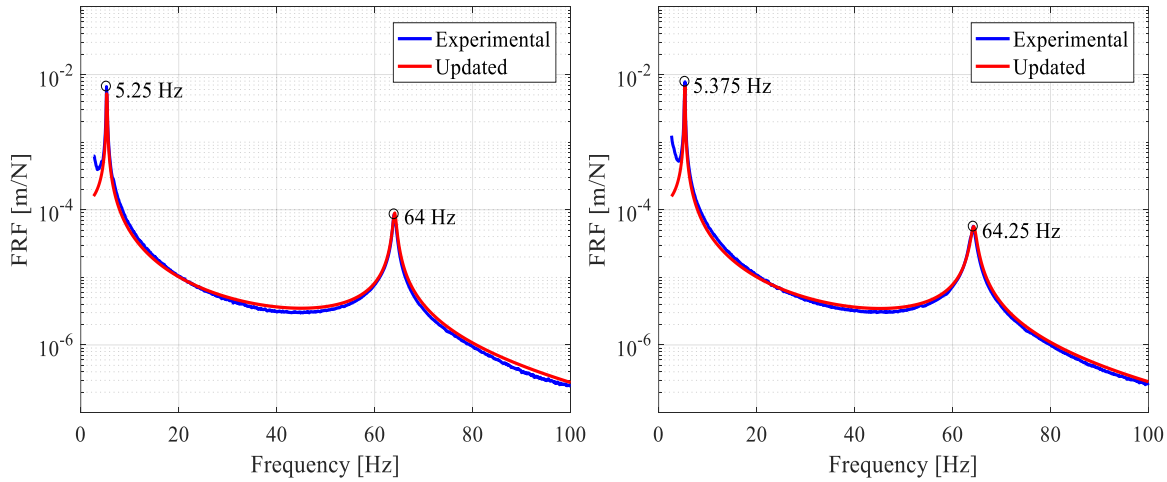

Figure 7. Numerical (updated 2D model) and experimental FRFs: (a) Impact forces along the *X* direction; (b) Impact forces along the *Z* direction.

Figure 8 shows the experimental FRFs considering the shaft with a 20% depth crack. It can be observed that the values of the natural frequencies remain equal to the ones obtained for the healthy shaft (see Fig. 7) (probably due to the frequency resolution used).

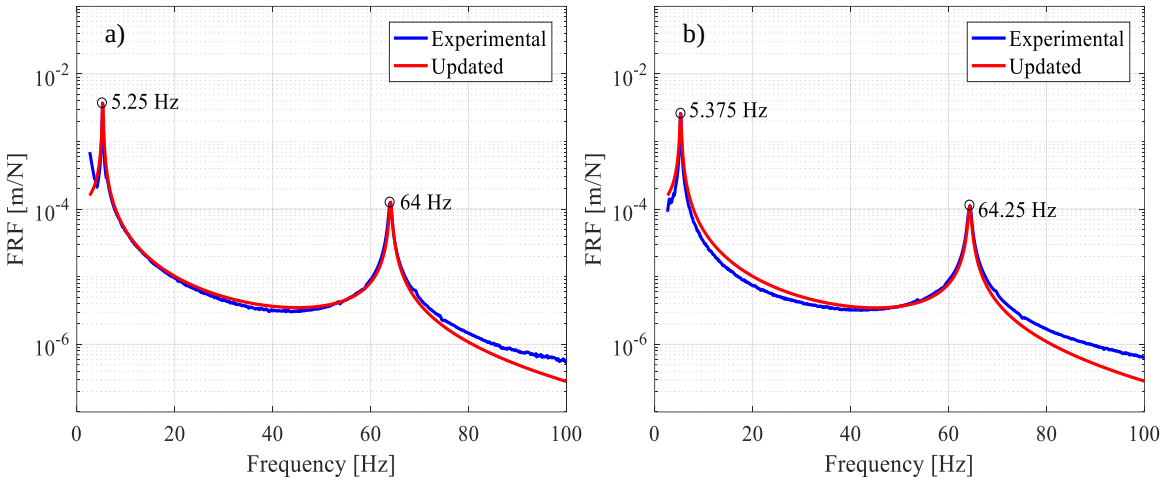

Figure 8. Numerical (updated 2D model) and experimental FRFs: (a) Impact forces along the X direction; (b) Impact forces along the Z direction.

Thus, a new damage configuration was evaluated considering the shaft with a 50% depth crack. The numerical and experimental FRFs obtained for this condition are shown in Fig. 9. In this case, a few changes are noted for the first natural frequency (2,38%). The influence of the crack on the second natural frequency of the system was not significant for the present condition.

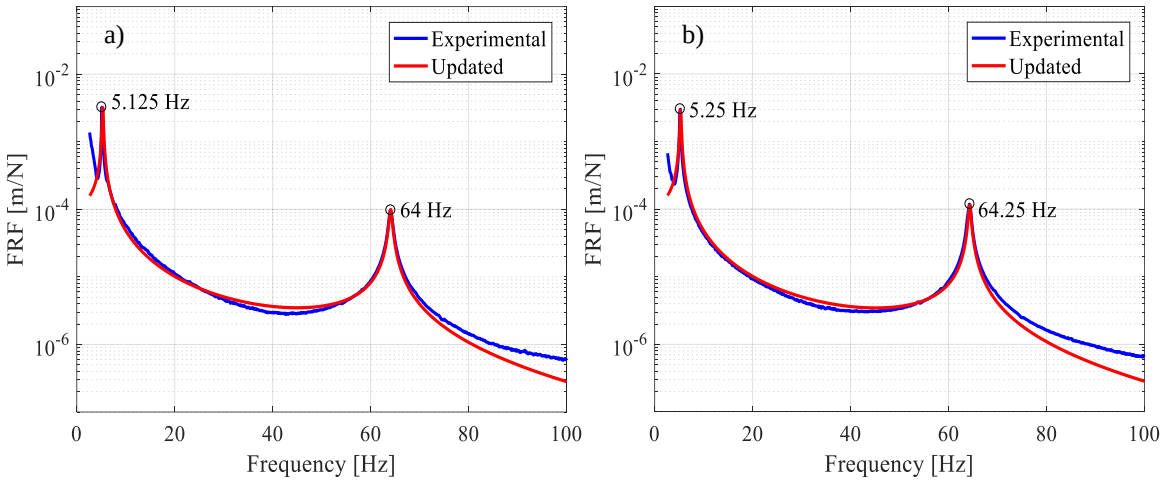

Figure 9: Numerical (updated 2D model) and experimental FRFs: (a) Impact forces along the X direction; (b) Impact forces along the Z direction

Figures 10, 11, and 12 shows the strain fields determined by using both the 2D and 3D models. The positions of the strain gauges presented in Fig. 2 were used as a reference. The damage conditions shown in Fig. 8 and Fig. 9 are considered. The numerical results were compared with the experimental data for different angular positions of the shaft. It is worth mentioning that the 2D model assumes linear stress and strain distribution.

Figure 10 shows the strain fields measured according to Fig. 2a for a 20% crack depth. It is possible to verify that the models are representative for this configuration. Note that there are many angular positions demonstrating satisfactory proximity of numerical and experimental results. This can be explained by the important influence of the linear behavior acting on this condition.

Figure 11 compares the results obtained by considering cracks with 20% and 50% depths using the strain gauge # 6 (see Fig. 2). Note that results obtained by using the 2D model are not satisfactory for the crack with 50% depth due to the nonlinear effects of the crack affecting the system on this condition. Better results were obtained by using the 3D

model as compared with the experimental measures, since both the nonlinear and the thermal strain effects were now activated in the analysis. Figure 12 shows the strain fields measured according to Fig. 2b for a 50% crack depth. It is possible to verify that models are quite representative for this configuration.

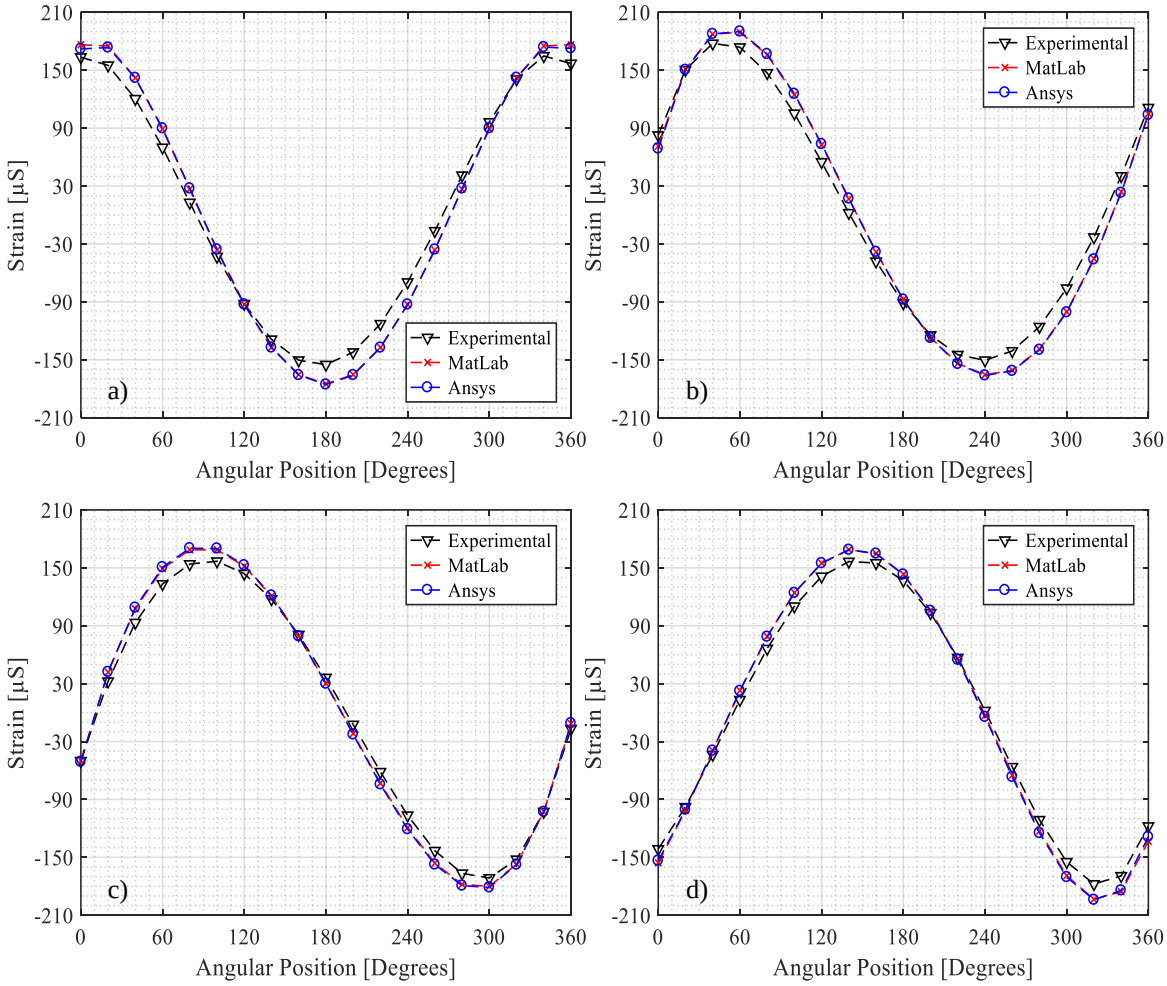

Figure 10. Comparison of calculated 2D and 3D strains with experimental results for 20% depth transversal crack: (a) Stain gauge 1; (b) Stain gauge 2; (c) Stain gauge 3; (d) Stain gauge 4

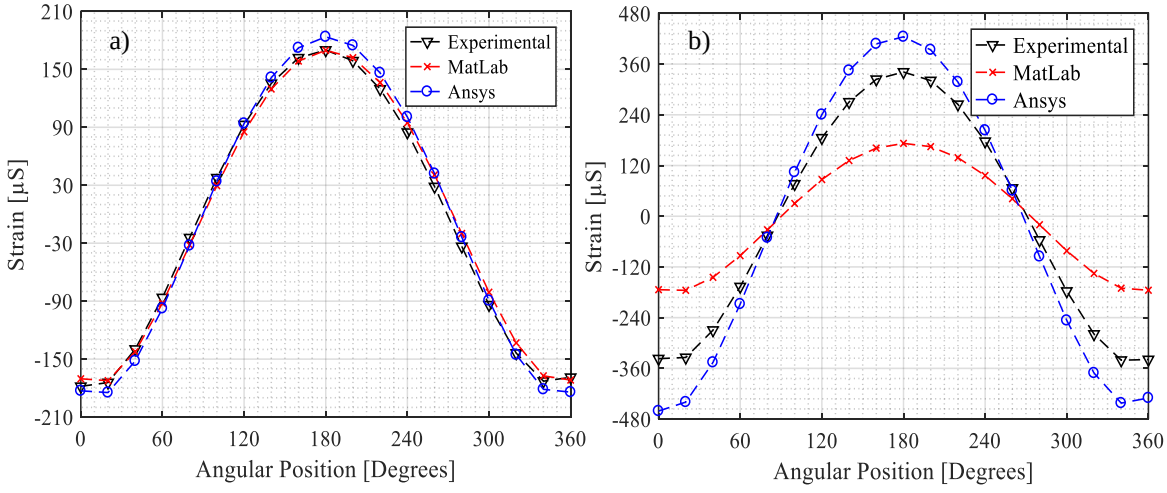

Figure 11. Comparison of calculated 2D and 3D strains with experimental results for strain gauge # 6: (a) 20% depth; (b) 50% depth;

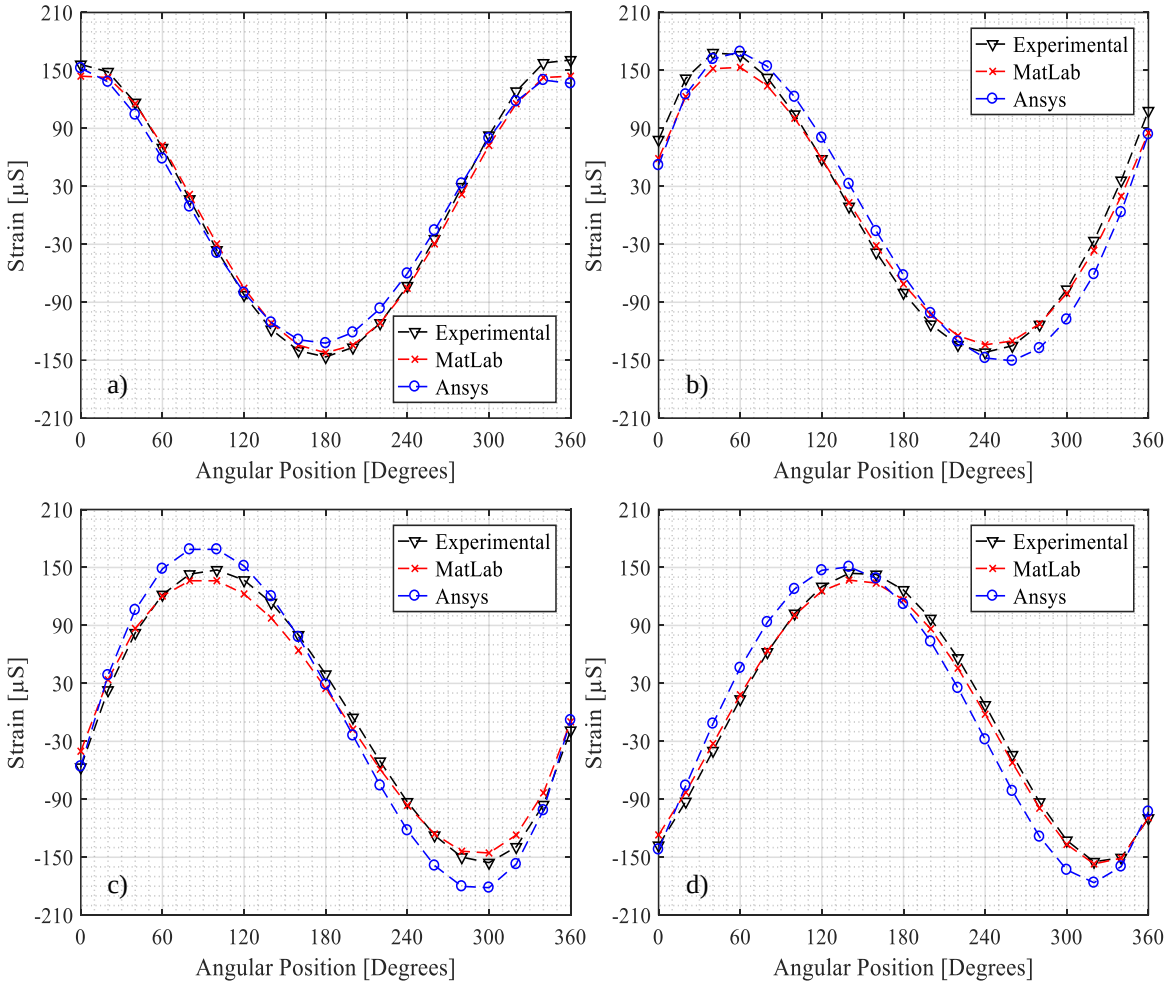

Figure 12. Comparison of calculated 2D and 3D strains with experimental results for 50% depth transversal crack: (a) Strain gauge #1; (b) Strain gauge #2; (c) Strain gauge #3; (d) Strain gauge #4

6. FINAL REMARKS

This work was dedicated to the investigation of the static and dynamic behavior of a cracked shaft both through numerical and experimental results. Firstly, the FRFs of the system were obtained for the following conditions: healthy shaft, 20%, and 50% crack depths. As expected, few changes were verified on the natural frequencies with the crack existence. The strain fields of the cracked shaft were measured experimentally in regions close to the crack position. The numerical results obtained by using 2D and 3D finite element models were presented for comparison purposes. Different angular positions of the shaft were analyzed. It was possible to observe that the 2D model is not able to represent the cracked shaft for deep cracks (for the other cases the model representation is considered adequate). Further research effort will be dedicated to include the rotordynamics effects on the considered analyses.

7. ACKNOWLEDGEMENTS

The authors are thankful to the Brazilian Research Agencies FAPEMIG, CNPq (INCT-EIE), and CAPES for the financial support provided to this research effort.

8. REFERENCES

Al-Shudeifat, M. A., 2013. *On the finite element modeling of the asymmetric cracked rotor*. Journal of Sound and Vibration.

Anderson, T. L., 2005. *Fracture Mechanics: Fundamentals and Applications*, Taylor & Francis, USA.

Bachschmid, N.; Pennacchi, P. and Tanzi, E., 2010. *Cracked rotors: a survey on static and dynamic behavior including modelling and diagnosis*, Springer.

Darpe, A.K.; Gupta, K. and Chawla A., 2004. *Coupled bending, longitudinal and torsional vibrations of a cracked rotor*. Journal of Sound and Vibration, Vol. 269, n. 1, p. 33-60.

Dimarogonas, A.D., 1996. *Vibration of cracked structures: a state of the art review*. Engineering Fracture Mechanics. Vol. 55, n. 5, p. 831-857.

Farrar, C.R.; Lieven, N.A.J. and Bement, M.T., 2005. "An Introduction to Damage Prognosis". In: Inman, D.J.; Farrar, C.R.; Lopes, V. and Steffen, V. (Eds.). *Damage Prognosis: For Aerospace, Civil and Mechanical Systems*, John Wiley & Sons Ltd, England, p. 1-12.

Gasch, R., 1976. Dynamic behaviour of a simple rotor with a cross sectional crack. In: *International Conference on Vibrations in Rotating Machinery*, IMechE, Vol. 1, n. 1, p. 123-128.

Mayes, I.W. and Davies, W.G.R., 1984. *Analysis of the response of multi-rotor-bearing system containing a transverse crack in a rotor*. Journal of Vibration, Acoustics, Stress, and Reliability in Design, Vol. 106, n. 1, p. 139-145.

Muszynska, A., 2005. *Rotordynamics*, Taylor & Francis Group,

Ostachowicz, W.M. and Krawczuk, M., 1992. *Coupled torsional and bending vibrations of a rotor with an open crack*. Arch. appl. Mech. 62, p. 191-201.

Papadopoulos, C.A., 2004. *Some comments on the calculation of the local flexibility of cracked shafts*. Journal of Sound and Vibration, Vol. 278, n. 1, pp. 1205–1211.

Papadopoulos, C.A. and Dimarogonas, A.D., 1987. *Coupled longitudinal and bending vibrations of a rotating shaft with an open crack*. Journal of Sound and Vibration, Vol. 117, n. 1, p. 81-93.

Papadopoulos, C.A. and Dimarogonas, A.D., 1989. "Coupled vibrations of cracked shafts". In: *ASME Design Technical Conferences, 12th Biennial Conference on Mechanical Vibration and Noise*. Quebec, p. 6-11.

Storn, R. and Price, K., 1995. *Differential evolution: a simple and efficient adaptive scheme for global optimization over continuous spaces*. International Computer Science Institute, Vol.12, n. 1, p. 1-16.

9. RESPONSIBILITY NOTICE

The authors are the only responsible for the printed material included in this paper.